Separation and Purification Technology 268 (2021) 118696

Contents lists available at ScienceDirect

Separation and Purification Technology

journal homepage: www.elsevier.com/locate/seppur

Sensitivity analysis of mass transfer and enhancement factor correlations for the absorption of CO_2 in a Sulzer DX packed column using 4-diethylamino-2-butanol (DEAB) solution

Peyman Pakzad [a], Masoud Mofarahi [a,b,*], Chang-Ha Lee [b]

[a] Department of Chemical Engineering, Faculty of Petroleum, Gas and Petrochemical Engineering, Persian Gulf University, Bushehr 75169, Iran
[b] Department of Chemical and Biomolecular Engineering, Yonsei University, 50 Yonsei-ro, Seodaemun-gu, Seoul 120-749, Republic of Korea

ARTICLE INFO

Keywords:
CO_2 capture
Packed column
Sensitivity analysis
Rate-based model
Sulzer DX

ABSTRACT

In this study, a rate-based model of post-combustion CO_2 capture was developed for an absorption column packed with Sulzer DX. A new amine solution, 4-diethylamino-2-butanol (DEAB), was applied to the absorber as an active CO_2 capture solvent, and a sensitivity analysis on mass-transfer coefficients in liquid and gas phases (k_L and k_G), effective interfacial area (a_e), and enhancement factor (E) correlations was conducted to enhance the performance of the absorber. In the modeling, the absorber was divided into two sections—low capacity (less than 0.5 mol CO_2/mol DEAB) and high capacity (more than 0.5 mol CO_2/mol DEAB)—to improve model prediction accuracy, especially at high CO_2 loading (α_{CO_2}). At α_{CO_2} of less than 0.5, the CO_2 equilibrium molar concentration ($C_{CO_{2,e}}$) was neglected, while at higher α_{CO_2}, the Deshmukh–Mather activity coefficient model was used to calculate $C_{CO_{2,e}}$. The solution procedure was validated against the axial experimental data of the CO_2 mole fraction in the gas phase (y_{CO_2}) and the liquid-phase temperature (T_L). Then, a sensitivity analysis was performed for the profiles of α_{CO_2}, y_{CO_2}, H_2O mole fraction in the gas phase (y_{H_2O}), T_L, and gas-phase temperature (T_G) through various mass-transfer correlations for the Sulzer DX packing. The rate-based model with k_L, k_G and a_e found that the correlation coefficient (R^2) and average absolute relative deviation ($AARD$%) of y_{CO_2} data were 0.9889 and 3.12, and those of T_L data were 0.9685 and 2.09. The sensitivity analysis of various E correlations also revealed no significant difference between the calculated E values using the different relationships. Finally, the effects of α_{CO_2}, T_L, and liquid flow rate (L) as the most important parameters of the absorber on the E value were investigated. The results indicated that α_{CO_2} has a significant impact on the E values and consequently on the reaction rate.

1. Introduction

1.1. Background

The Intergovernmental Panel on Climate Change (IPCC) reported that the contribution of human activities to global warming reached approximately 1 °C over the pre-industrial level in 2017 [1]. The global warming rate may increase up to 1.5 °C from 2030 to 2052. As a greenhouse gas, CO_2 contributes to more than 60% of global climate change [2]. The combustion of fossil fuels in the thermal power plants is the primary source of emissions of this gas in the environment. CO_2 removal is conducted through various technologies such as adsorption, absorption, membranes systems, cryogenics techniques, and microbial systems [3]. Currently, acid gas absorption into an aqueous amine solution is one of the most affordable and effective technologies for removing CO_2 from the industrial gas streams [4]. The process design, absorbent, and column packing are essential to this technology [5]. An effective and advanced absorbent can significantly enhance CO_2 capture performance [6].

Conventional solvents used for the CO_2 capture include amines or alkanolamines, which chemically react with CO_2 in an absorption column and then desorb the collected CO_2 in a stripper or desorption column. Recycling of the recreated amine solution to the absorption column is then performed [7]. The most well-known amines for removing CO_2 on an industrial scale are diethanolamine (DEA), monoethanolamine (MEA), 2-amino-2-methyl-1-propanol (AMP), methyldiethanolamine (MDEA), and piperazine (PZ) [8,9].

* Corresponding author.
E-mail address: mofarahi@pgu.ac.ir (M. Mofarahi).

https://doi.org/10.1016/j.seppur.2021.118696
Received 19 January 2021; Received in revised form 28 March 2021; Accepted 29 March 2021
Available online 2 April 2021

Nomenclature

a	specific surface area of packing (m^2/m^3)
a_e	effective interfacial area of packing (m^2/m^3)
$AARD$	average absolute relative deviation (%)
$C_{CO_2,e}$	CO_2 equilibrium molar concentration (kmol/m^3)
$C_{CO_2,i}$	CO_2 molar concentration at the gas–liquid interface (kmol/m^3)
C_{DEAB}	DEAB concentration (kmol/m^3)
C_{P,CO_2}	CO_2 molar heat capacity (kJ/kmol K)
$C_{P,G}$	gas molar heat capacity (kJ/kmol K)
C_{P,H_2O}	H_2O molar heat capacity (kJ/kmol K)
$C_{P,L}$	liquid molar heat capacity (kJ/kmol K)
dZ	differential packed height
$D_{CO_2,L}$	diffusivity of CO_2 in liquid (m^2/s)
$D_{DEAB,L}$	diffusivity of DEAB in liquid (m^2/s)
$D_{G,ave}$	average diffusion coefficient in gas phase (m^2/s)
E	enhancement factor
E_∞	enhancement factor for instantaneous reaction
G	gas flow rate (kmol/m^2 s)
h	heat transfer coefficient (J/m^2 s K)
H_{CO2}	henry's constant of CO_2 (kPa m^3/K mol)
Ha	Hatta number
k_2	second-order reaction rate constant (m^3/kmol s)
K_i	chemical reaction equilibrium constants (MPa kg/mol)
k_g	gas phase mass transfer coefficient (kmol/m^2 kPa s)
$k_{G,ave}$	average gas phase mass transfer coefficient (kmol/m^2 kPa s)
k_l	liquid phase mass transfer coefficient (m/s)
k_L^0	ordinary liquid phase mass transfer coefficient (m/s)
L	liquid molar flow rate (kmol/m^2 s)
$M_{w,ave}$	average molecular weight of gas phase ()
N_{CO_2}	molar flux of CO_2 (kmol/m^2 s)
N_{H_2O}	molar flux of H_2O (kmol/m^2 s)
P	total pressure of gas phase (kPa)
q	heat flux (J/m^2 s)
R	general gas constant (kPa m^3/kmol K)
R^2	correlation coefficient
T_G	gas phase temperature (K)
T_L	liquid phase temperature (K)
x_{CO_2}	CO_2 mole fraction in liquid phase
x_{H_2O}	H_2O mole fraction in liquid phase
y_{CO_2}	CO_2 mole fraction in gas phase
$y_{CO_2,i}$	CO_2 mole fraction at the gas–liquid interface
y_{H_2O}	H_2O mole fraction in gas phase

Greek symbols

α_{CO_2}	CO_2 loading (mol CO_2/mol DEAB)
ΔH_{CO_2}	heat of absorption of CO_2
ΔH_{H_2O}	heat of vaporization of H_2O
ε	void fraction of packing (m^3/m^3)
γ_i	activity coefficient of component$i$
λ_G	thermal conductivity of gas phase (J/m K s)
θ	crimp angle of packing (°)
μ_G	viscosity of gas phase (kg/m s)
μ_L	viscosity of liquid phase (kg/m s)
ρ_G	density of gas phase (kg/m^3)
ρ_L	density of liquid phase (kg/m^3)
σ_L	surface tension of liquid (N/m)
φ_{CO_2}	fugacity coefficient of CO_2

Superscripts

G	Gas
i	Interface
L	Liquid

Due to the demands for further enhancement of CO_2 capture efficiency, many studies have been conducted to develop novel amines with suitable features (high absorption rate and capacity, low corrosion and degradation tendencies, and high mass-transfer performance) [10]. Innovative amino alkol solvents were developed to capture CO_2 from industrial gas streams more effectively than conventional solvents [11]. Based on evaluating nine different solvents, 4-diethylamino-2-butanol (DEAB), a tertiary amine, had the highest cyclic capacity. DEAB has an absorption capacity comparable with PZ and higher than those of MDEA, DEA, AMP, and MEA [12]. Furthermore, the cyclic capacity of DEAB is higher than MEA and MDEA. Furthermore, a lower operating cost and circulation rate have been reported for DEAB [13] because the regeneration of DEAB requires lower energy than that of MEA, MDEA, and DEA [12,14].

The reaction rate constant of DEAB is comparable with AMP and DEA, which is higher than that of MDEA and lower than that of MEA and PZ. Moreover, the total mass-transfer coefficient ($K_G a_v$) of CO_2 into DEAB solution is greater than that in MDEA but smaller than MEA [15]. Moreover, DEAB possesses lower viscosity at 298 K that MDEA and MEA [16]. Consequently, DEAB should have high potential as an alternative solvent for the absorption of CO_2 to replace conventional amines, especially to substitute tertiary amines such as MDEA.

The contact efficiency between the liquid and gas phases in an absorber is crucial in a CO_2 absorption process. In recent decades, tray columns have been widely replaced by packed columns [17]. The suitable packing exhibits a low pressure drop along the absorber, a high surface area-to-volume ratio, and uniform distribution in the contact area between gas and liquid where the liquid stream is broken into droplets. In the absorber, mass- and heat-transfer operations rely on the properties of the absorbent and packing [17,18].

Because the enhanced liquid surface area leads to increased contact with the gas phase, the absorption rates can be improved. Structured packing materials produce greater CO_2 absorption than random packing materials [19,20]. DX packing, one of the primary types of modern structured packing from Sulzer Chemtech CANADA, Inc., may enhance the absorption performance for CO_2 capture because of its high surface area (900 m^2/m^3), low height of equivalent theoretical stages (HETP), coarse structure, low pressure drop, and easy fabrication with fewer parts [21,22]. Consequently, there is significant demand for reliable models to evaluate the mass-transfer performance in structure packing materials.

1.2. Literature review

Much literature exists regarding the simulation and process modeling of CO_2 absorption within packed columns. According to previous studies [23], the modeling methods developed thus far differ in selecting kinetic and thermodynamic models for appropriate heat and mass transfer. The absorber column can be modeled by an infinite number of mass transfer stages which every one represents a part of packing performance in the column. It is possible to model each stage through a rate-based or equilibrium-stage model, where vapor–liquid equilibrium is presumed at the interface. A rate-based model allows us to model an absorption column by an arbitrary number of finite stage with considering mass- and heat-transfer restrictions[24]. For chemisorption procedures with fast reaction kinetics, similar to the considered

procedure, a rate-based procedure is more reliable [25]. Comparative studies were conducted for the two methods using the same thermophysical property model for absorption of CO_2 into AMP [26] and MEA [27] solutions, respectively. Moreover, the rate-based model presented a more precise explanation of the pilot-plant composition and temperature profiles.

The use of a rate-based method requires appropriate treatment of heat- and mass-transfer phenomena. In a two-film model, the temperature and concentration profiles across hypothetical films can be imposed by considering the effects of chemical reactions on mass-transfer with an enhancement factor (E), which is defined as the ratio of absorption rate with reaction relative to that without reaction [28]. The E alters along the length of the column length and can be frequently set to the pilot-plant information, which is followed in most CO_2 absorption models [23,29].

The mass-transfer coefficients are required in all rate-based models to consider the type of used packing and the operating circumstances. Various semi-theoretical or empirical mass-transfer correlations for structured packing have been published [30]. Furthermore, semi-empirical or reliable empirical efficiencies for specific products from packing suppliers can be found in their product bulletins. Such models were examined against several pilot plant data sources with various limitations, precisions, and suitability ranges for use [30]. Thus, the proper choice of a packing mass-transfer correlation is essential for precise absorber design [30–32].

In modeling CO_2 absorbers, another critical concern is representing the fluid phase equilibria and chemical reactions of the mixture of H_2O, CO_2, and amine. Two classes for the thermodynamic model of liquid and gas phases in the absorber are conventionally applied for chemical reaction equilibria. The first class is non-rigorous models, assuming that the activity coefficients of all the species existing in the equilibrium reactions are equal to unity and the equilibrium constants are the adjustable parameters. Non-rigorous models, such as those by Kent-Eisenberg [33] and Gabrielsen [34], have been commonly adopted in recent years with rate-based models [23,35]. However, a weak extrapolation capacity is the primary limitation of this class [36].

The second class is the rigorous method, in which an equation of state (EoS) considers the non-ideality of the vapor phase, and an activity coefficient model considers the non-ideality of the liquid phase. The Deshmukh–Mather model [37], Austgen model [38], Pitzer's activity model [39], electrolyte NRTL model [39], and extended UNIQUAC model [39] could be used as activity coefficient models. The primary disadvantage of such models is the presence of several parameters, requiring ample experimental information for reaction kinetics and vapor–liquid equilibrium (VLE) [40]. The Austgen model has been widely used [23], and the Deshmukh–Mather model has been successfully incorporated with the rate-based model for a CO_2 absorber using a randomly packed column using 1DMA2P solution [41].

Simulation and modeling are essential for understanding and evaluating the performance of the CO_2 absorption process and its scale-up using novel or advanced absorbents. The efforts have been concentrated on the performance of aqueous MEA and AMP solutions due to their extensive industrial use and pilot-plant data availability [25]. According to the literature, no study was conducted on the simulation and rate-based modeling of CO_2 packed-bed absorbers using new amines because of insufficient information for their thermophysical features. The purpose of this study is described in the next section.

1.3. Novelty of the work

The primary objectives of this study are as follows:

(1) The first rate-based model was extended to describe the composition and temperature profiles in a Sulzer DX packed absorber with DEAB solution.
(2) The most important single source of deviation between rate-based model results and experiments is equilibrium, especially at higher loadings [42]. Furthermore, the numerical solution of a rate-based model requires significant time to simulate an absorption column. In this study, the packed column was divided into two sections to accelerate the simulation time with accuracy. In the first section (i.e., at the top of the column) where the CO_2 loading (α_{CO_2}) value was less than 0.5 mol CO_2/mole DEAB, the CO_2 equilibrium molar concentration ($C_{CO_{2,e}}$) value was neglected. In contrast, in the second section (i.e., at the bottom of the column), the α_{CO_2} value was larger than 0.5 mol CO_2/mole DEAB. The value of $C_{CO_{2,e}}$ was estimated by the Deshmukh–Mather model. The computation of $C_{CO_{2,e}}$ could then be simplified by this strategy in the bulk liquid-phase over a high α_{CO_2} range.
(3) The sensitivity analysis of various mass-transfer coefficients in liquid and gas phases (k_L and k_G) and effective interfacial area (a_e) correlations, specifically proposed for Sulzer DX packing in

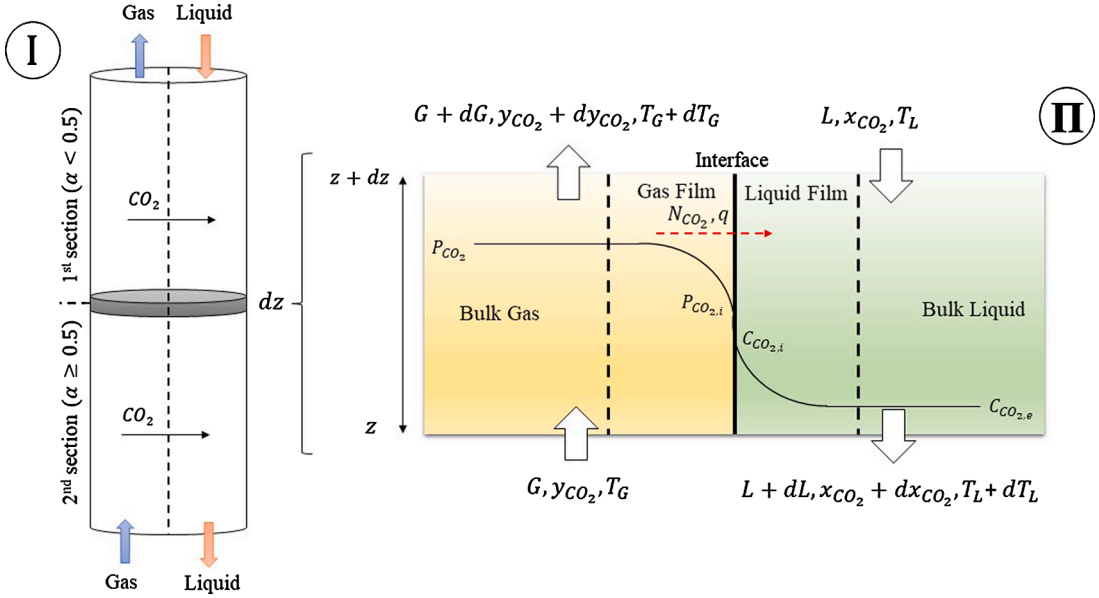

Fig. 1. Illustration of the gas and liquid mass transfer occurring in the differential packed height (dZ) during the absorption process.

the literature, was conducted comprehensively through the rate-based model.

(4) With the k_L, k_G, and a_e, correlations selected from the sensitivity analysis, the effect of five different E correlations on the rate-based model was investigated. Furthermore, the effects of α_{CO_2}, liquid-phase temperature (T_L), and liquid flow rate (L) on the calculated E values were studied.

The experimental data of y_{CO_2} and T_L profiles from the Sulzer DX packed CO_2 absorber using the DEAB solution were measured from the pilot-plant runs of Naami [43] to validate the model. The developed rate-based model, containing material and energy balance equations, all correlations used in sensitivity analysis, E models, and Deshmukh–Mather model [37], were implemented using MATLAB® software.

2. Rate-based model

The first steady-state rate-based method was presented by modeling chemical CO_2 absorption reactions with aqueous MEA solution [44]. The enthalpy balances and differential mass were adjusted, and the ideal solution and gas for describing the liquid and gas phases were used. Because an obvious expression for the E led to a boundary value problem, it was solved via a shooting technique. Constant liquid and gas flow rates were presumed along the packed column. In this study, the rate-based model for DEAB solution was modified with the following assumptions:

- The absorber, based on the amount of α_{CO_2}, was split into two sections because this strategy could save computation time without accuracy loss.
- The equations of the liquid and gas flow rates throughout the column were engaged for flow rate changes in the computational model.
- Both the liquid and gas phases are non-ideal. Accordingly, the Peng-Robinson EOS and Deshmukh-Mather thermodynamic model were applied for the gas- and liquid-phase non-ideal behavior.
- The effect of solvent evaporation was negligible.
- An evaluation to select the proper correlations of a_e, k_L, k_G, and E was conducted for the Sulzer DX packing.

The model maintains the two-film theory assumptions for the CO_2-DEAB-H_2O system in the Sulzer DX packed column to derive the governing equations.

2.1. Material and energy balances

Fig. 1. presents the schematics of the differential elements required for the conservation equation through the length of the column. Envelopes II depicts an infinitesimal volume within the differential packed height (dZ) of the column containing the liquid and gas phases. The diffusion of CO_2 molecules occurs in the liquid phase while the reaction with DEAB solution produces nonvolatile products. Interfacial mass- and heat-transfer and thermophysical properties of each phase are considered with the assumptions to establish the group of equations. The key hypotheses of the model are:

- The reaction is rapid and occurs in the liquid phase.
- The absorption column is insulated, and the reaction occurs adiabatically.
- The interfacial surface areas for both mass- and heat-transfer are identical.
- A heat-transfer resistance in the liquid phase is smaller than that in the gas phase. Therefore, the bulk and interface temperatures are identical.
- Variation in temperature and concentration is negligible in a radial direction.

The energy and material balances applied to the dZ produced Eqs. (1) to (8).

- Material balance equations:

$$\frac{dG}{dz} = -(N_{CO_2} + N_{H_2O})a_e \tag{1}$$

$$\frac{dy_{CO_2}}{dz} = \frac{\left[N_{CO_2}\left(y_{CO_2} - 1\right) + N_{H_2O}y_{CO_2}\right]a_e}{G} \tag{2}$$

$$\frac{dy_{H_2O}}{dz} = \frac{\left[N_{H_2O}\left(y_{H_2O} - 1\right) + N_{CO_2}y_{H_2O}\right]a_e}{G} \tag{3}$$

$$\frac{dL}{dz} = -N_{H_2O}a_e \tag{4}$$

$$\frac{dx_{CO_2}}{dz} = \frac{(N_{H_2O}x_{CO_2} - N_{CO_2})a_e}{L} \tag{5}$$

$$\frac{dx_{H_2O}}{dz} = \frac{[N_{H_2O}(x_{H_2O} - 1) + N_{CO_2}]a_e}{L} \tag{6}$$

where$L$ and G are the liquid and gas flow rates, N_{CO_2} and N_{H_2O} are the CO_2 and H_2O molar flux from gas to liquid, a_e is the effective interfacial area of packing per volume, y_{CO_2} and y_{H_2O} are the CO_2 and H_2O mole fractions in the gas phase, and x_{CO_2} and x_{H_2O} are the total CO_2 and H_2O mole fractions in the liquid phase. $N_{CO_2}$is neglected in Eq. (4) from the liquid phase mass balance because the reacted CO_2 does not alter the total number of moles.

Energy balance equations:

$$\frac{dT_G}{dz} = -\frac{qa_e}{GC_{P,G}} \tag{7}$$

$$\frac{dT_L}{dz} = -\frac{qa_eA_c}{LC_{P,L}} + \frac{\left(N_{CO_2}C_{P,CO_2} + N_{H_2O}C_{P,H_2O}\right)a_e(T_L - T_G)}{LC_{P,L}} + \frac{(N_{CO_2}\Delta H_{CO_2} + N_{H_2O}\Delta H_{H_2O})a_e}{LC_{P,L}} \tag{8}$$

where T_L and T_G are the liquid and gas temperatures, $C_{P,G}$, $C_{P,L}$, C_{P,CO_2}, and C_{P,H_2O} are the liquid, gas, CO_2, and H_2O molar heat capacities, ΔH_{CO_2} is the heat of absorption of CO_2, ΔH_{H_2O} is the heat of vaporization of H_2O, and q is the heat flux from gas to liquid. The Chilton–Colburn analogy is used to calculate the heat-transfer coefficient (h) between the gas and liquid phases [45].

$$q = h(T_G - T_L) \tag{9}$$

$$h = k_{G,ave}RT_G\left(\frac{C_{P,G}\rho_G}{M_{w,ave}}\right)^{\frac{1}{3}}\left(\frac{\lambda_G}{D_{G,ave}}\right)^{\frac{2}{3}} \tag{10}$$

where $k_{G,ave}$ is the average gas-phase mass-transfer coefficient, R is the universal gas constant, ρ_G is the gas density, $M_{w,ave}$ is the average molecular weight of the gas phase, λ_G is the thermal conductivity of the gas

Table 1
Correlations for the liquid and gas phase mass transfer coefficients (k_L and k_G) and the effective interfacial area (a_e) for Sulzer DX packing.[a]

Case	Correlation	Reference
	$\frac{a_e}{a_p} = 921\left(\frac{We_L Fr_L}{Re_L}\right)^{\frac{2}{3}}\left(\frac{u_G}{u_L}\right)$	Gao et al. [21]
Case A	$k_G =$ $0.054\left(\frac{D_{CO_2,G}}{S}\right)\left(\frac{(U_{Ge}+U_{Le})\rho_G S}{\mu_G}\right)^{0.8}\left(\frac{\mu_G}{D_{CO_2,G}\rho_G}\right)^{0.33}$	Rocha et al. [51,52]
	$k_L = 2\sqrt{\frac{0.9 D_{CO_2,L} U_{Le}}{\pi S}}$	Rocha et al. [51,52]
	$\frac{a_e}{a_p} = 2.308 Re_G^{-0.274} Re_L^{0.246} We_L^{0.248} Fr_L^{-0.161}$	Hanley and Chen [50]
Case B	$k_G = 0.3516 Re_G^{\frac{1}{2}} Sc_G^{\frac{1}{3}}\left(\frac{c_G D_{CO_2,G}}{d_h}\right)$	Hanley and Chen [50]
	$k_L = 12 Re_L^{1} Sc_L^{\frac{1}{3}}\left(\frac{c_L D_{CO_2,L}}{d_h}\right)$	Hanley and Chen [50]
	$\frac{a_e}{a_p} = 0.759 Re_L^{0.254}$	De Montigny et al. [47]
Case C	$k_G = 0.0338\left(\frac{D_{CO_2,G}}{d_h}\right)\left(\frac{u_G \rho_G d_h}{\mu_G \cos\theta}\right)^{0.8}\left(\frac{\mu_G}{D_{CO_2,G}\rho_G}\right)^{0.33}$	Henriques de Brito et al. [49]
	$k_L = \sqrt{D_{CO_2,L} sr}$	Cho [77]

[a] Change of $D_{CO_2,G}$ to $D_{H_2O,G}$ in $k_G$equations yields an expression analogous for k_G of H_2O.

phase, and $D_{G,ave}$ is the average diffusion coefficient in the gas phase.

2.2. Interfacial mass transfer

The N_{CO_2} that crosses the gas–liquid interface is explained by the total gas mass-transfer expression.

$$N_{CO_2} = k_G P\left(y_{CO_2} - y_{CO_2,i}\right) = Ek_L^0\left(C_{CO_2,i} - C_{CO_{2,e}}\right) \tag{11}$$

where $y_{CO_2,i}$ is the CO_2 mole fraction at the gas–liquid interface, $C_{CO_2,i}$ is the CO_2 molar concentration at the gas–liquid interface, and P is the total pressure of the gas phase. E is the ratio between k_L and the ordinary liquid-phase mass-transfer coefficient (k_L^0). Its quantity is either greater than or equal to 1.0, based upon the reaction trend [46]. The $C_{CO_2,i}$ can be estimated using Henry's law (Eq. (12)).

$$C_{CO_2,i} = \frac{P y_{CO_2,i} \varphi_{CO_2}}{H_{CO_2} \gamma_{CO_2}} \tag{12}$$

where φ_{CO_2} is the fugacity coefficient of CO_2, H_{CO_2} is the Henry's constant of CO_2 in DEAB solution, and γ_{CO_2} is the activity coefficient of CO_2. Substitution of Eq. (12) into Eq. (11) produces the following expression:

$$y_{CO_2,i} = \frac{y_{CO_2} + \frac{1}{P}\left(\frac{Ek_L^0}{k_G}\right) C_{CO_{2,e}}}{1 + \frac{\varphi_{CO_2}}{\gamma_{CO_2} H_{CO_2}}\left(\frac{Ek_L^0}{k_G}\right)} \tag{13}$$

The computation of $y_{CO_2,i}$ differs in each column section. In the second section, when the loading value is more than 0.5 mol CO_2/mol DEAB, $C_{CO_{2,e}}$ in the liquid bulk is significant and cannot be ignored [35]. Hence, in the second section of the column, Eq. (13) is used to calculate $y_{CO_2,i}$. In the first section of the column, $C_{CO_{2,e}}$ in the liquid bulk is very small because the loading value is restricted up to 0.5 mol CO_2/mol DEAB [16,23,35]. Thus, it can be neglected in calculating the first column section. Then, Eq. (13) is simplified to Eq. (14).

$$y_{CO_2,i} = \frac{y_{CO_2}}{1 + \frac{\varphi_{CO_2}}{\gamma_{CO_2} H_{CO_2}}\left(\frac{Ek_L^0}{k_G}\right)} \tag{14}$$

2.3. k_L ,k_G, and a_e correlations

k_L, k_G, and a_e are the key design factors in the rate-based determination of CO_2 absorption through amine solutions in packed columns. The parameters indicate the absorber performance presented in Eq. (11) for calculating the liquid and gas phase mass-transfer rates within the rate-based model.

Some correlations of k_L, k_G, and a_e for the structured packing column of the Sulzer DX type are available in the literature. The CO_2 capture from a Sulzer DX packed column using aqueous MEA solution was investigated [47] using a basic computer model [48] with a modification of a_e correlation [49]. In this study, the correlations were also developed for the DX structured packing columns using DEAB solution. Later, a comprehensive modeling study was conducted by assessing various k_L, k_G, and a_e correlations such as complex and simple models for the structured packing (Sulzer DX) and random packing (IMTP 40 and pall rings) via CO_2 capture in MDEA, AMP, and MEA solutions [32]. The k_L, k_G, and a_e correlations [50] provided accurate estimations of the experimental data among various correlations.

An experimental hydrodynamic study for the Sulzer DX structure packing suggested a simple a_e correlation [21]. When this correlation was used together with the k_L and k_G correlations [51,52], the simple a_e correlation revealed high consistency for the modeling of the packed column in the Sulzer DX structure packing [53]. Hence, the reported k_L and k_G correlations [51,52] and a_e correlation [21] were also used in this study for the Sulzer DX packed column. The correlations depend on the system specification, limitation, and accuracy. Therefore, the sensitivity analysis of various k_L, k_G, and a_e correlations were conducted using the rate-based model to assess the suitable correlations for simulation and

Table 2
Different Enhancement Factor (E) correlations used this study.[a]

Case	Equations	Description	Reference
Case 1	$E = Ha$	Pseudo 1st first order reaction	Danckwerts [57]
Case 2	$E = 1 + (E_2 - 1)\left\{1 - exp\left[-\frac{(Ha-1)}{(E_2-1)}\right]\right\}$	Explicit form 2nd order reactions	Porter [60]
Case 3	$E = 1 + \frac{1}{\left[\left(\frac{1}{E_\infty - 1}\right)^{1.35} + \left(\frac{1}{E_1 - 1}\right)^{1.35}\right]^{\frac{1}{1.35}}}$	Explicit form 2nd order reactions	Wellek et al. [61]
Case 4	$E = \frac{E_1^2}{2(E_\infty - 1)}\left(\sqrt{1 + \frac{4E_\infty(E_\infty - 1)}{E_1^2}} - 1\right)$	Explicit form 2nd order reactions	Yeramian et al. [62]
Case 5	$E = \left[\left(1 + \frac{n^{\overline{(n-1)}}(E_\infty - 1)^{\overline{(n-1)}}E_\infty}{(1+Ha^2)^{\overline{(2n-2)}}}\right) - 1\right]^{\frac{1}{n}} \times \frac{(1+Ha^2)^{\overline{(2n-2)}}}{n^{\overline{(n-1)}}(E_\infty - 1)^{\overline{(n-1)}}}$, with $n = 2$	Explicit form reversible reactions	Astarita et al. [63]

[a] where $Ha = \frac{\sqrt{k_2 C_{DEAB} D_{CO_2,L}}}{k_L^0}$, $E_\infty = 1 + (\frac{C_{DEAB} D_{DEAB}}{2 D_{CO_2,L} C_{CO_2,i}})$, $E_1 = \frac{\sqrt{Ha}}{\tanh\sqrt{Ha}}$,$E_2 = \sqrt{\frac{D_{CO_2,L}}{D_{DEAB}}} + \sqrt{\frac{D_{DEAB}}{D_{CO_2,L}}}\left(\frac{C_{DEAB}}{2C_{CO_2,i}}\right)$.

Table 4
The optimized interaction parameters in the Deshmukh-Mather model for the CO_2 + DEAB + H_2O system [67].

β_{ij}	a_{ij}	b_{ij}
$\beta_{DEABH^+-CO_2}$	−2.18	−1.50
$\beta_{DEABH^+-HCO_3^-}$	2.07	4.60
$\beta_{DEABH^+-CO_3^{2-}}$	−8.35	−5.01
$\beta_{DEAB-CO_2}$	−3.40	−3.52
$\beta_{DEAB-HCO_3^-}$	10.75	−0.64
$\beta_{DEAB-CO_3^{2-}}$	−3.61	−1.11
$\beta_{CO_2-HCO_3^-}$	−5.25	19.49
$\beta_{CO_2-CO_3^{2-}}$	0.67	−5.32

modeling of the Sulzer DX packed column used in this study. All applied correlations are summarized in Table 1 (Cases A-C).

2.4. *E* Correlations

The estimation of the liquid phase resistance against mass-transfer is essential for understanding its effects on chemical reactions. This effect is normally stated in terms of *E*, determined as the ratio of the absorption rate with chemical reactions to the rate with no chemical reactions [54]. The reactions between CO_2 and DEAB are either fast or instantaneous [55]. Depending upon the mass-transfer theory and the absorption rate, several *E* expressions are developed as functions of the Hatta number, based on the well-established two-film theory [56].

More complex correlations were also reported related to the penetration and surface-renewal theories [57,58]. An implicit correlation for *E* was developed in terms of the two-film theory model for an irreversible second order reaction [59]. However, due to numerical difficulties of implicit equations at high enhancement factors for an instantaneous reaction (E_∞), the explicit expressions for *E* are favored in modeling [23].

Danckwerts [57] provided several correlations of *E* for various kinds of chemical reactions. Various explicit correlations for *E* were suggested using a second-order irreversible reaction [60] and a two-film theory [61]. Another explicit *E* expression [62] was established by a second-order irreversible reaction through generalization to surface-renewal and penetration theories [59]. A correlation considering an instantaneous reversible chemical reaction was also proposed [63], which includes a constant variable *n* to explain the smoothness of the transition of CO_2 from the gas phase to the liquid phase.

In this study, five different explicit expressions of *E*, which are more commonly used in the literature, are considered to examine their effects on the model and simulation of Sulzer DX packed columns using a rate-based model (Table 2).

The second-order reaction rate constant (k_2) between DEAB and CO_2 in *E* equations is approximated from the following correlation [55].

$$k_2 = 4.01 \times 10^{13} \exp\left(\frac{-7527.7}{T}\right) \tag{15}$$

2.5. Thermodynamic modeling

$C_{CO_{2,e}}$ is approximated using the Deshmukh-Mather thermodynamic model [37]. The model, oriented by the $\gamma-\varphi$ method, predicted successfully the α_{CO_2} values and equilibrium species in the liquid phase [64,65]. DEAB as a tertiary amine solvent refunctions as a base catalyst to hydrate CO_2 [66]. The total reaction of DEAB solvent to capture CO_2 occurs as the following reactions [12,13,16,67].

$$DEABH^+ \overset{K_1}{\leftrightarrow} DEAB + H^+ \tag{16}$$

Table 3
The parameters for equilibrium constants (K_i) of Eq. (27) (based on molar concentration).

K_i	*A*	*B*	*C*	*D*	Reference
K_1	−4908.0	0.0008	0.0033	−4.0987	Afkhamipour and Mofarahi [67]
K_3	−12092.1	−36.7816	0.0000	235.482	Edwards et al. [78]
K_4	−12431.7	−35.4819	0.0000	220.067	Edwards et al. [78]
K_5	−13445.9	−22.4773	0.0000	140.932	Edwards et al. [78]

$$CO_2 + DEAB + H_2O \overset{K_2}{\leftrightarrow} DEABH^+ + HCO_3^- \tag{17}$$

$$CO_2 + H_2O \overset{K_3}{\leftrightarrow} HCO_3^- + H^+ \tag{18}$$

$$HCO_3^- \overset{K_4}{\leftrightarrow} CO_3^{2-} + H^+ \tag{19}$$

$$H_2O \overset{K_5}{\leftrightarrow} OH^- + H^+ \tag{20}$$

The chemical reaction equilibrium constants (K_i), which are equivalent to the reactions (Eqs. (16)–(20)), are:

$$K_1 = \frac{[H^+][DEAB]}{[DEABH^+]} \frac{\gamma_{H^+}\gamma_{DEAB}}{\gamma_{DEABH^+}} \tag{21}$$

$$K_2 = \frac{[DEABH^+][HCO_3^-]}{[CO_2][DEAB]} \frac{\gamma_{DEABH^+}\gamma_{HCO_3^-}}{\gamma_{CO_2}\gamma_{DEAB}} = K_1 K_3 \tag{22}$$

$$K_3 = \frac{[H^+][HCO_3^-]}{[CO_2]} \frac{\gamma_{H^+}\gamma_{HCO_3^-}}{\gamma_{CO_2}} \tag{23}$$

$$K_4 = \frac{[H^+][CO_3^{2-}]}{[HCO_3^-]} \frac{\gamma_{H^+}\gamma_{CO_3^{2-}}}{\gamma_{HCO_3^-}} \tag{24}$$

$$K_5 = [H^+][OH^-] \tag{25}$$

where $[i]$ and γ_i are the molality of species and equivalent activity coefficients. K_i for each reaction as a function of temperature is:

$$\ln(K_i) = \frac{A}{(T)} + B\ln(T) + C(T) + D \tag{26}$$

The parameters, *A*, *B*, *C*, and *D* are summarized in Table 3. The γ_i values of the chemical species are determined in terms of the extended Debye–Hückel equation in the Deshmukh–Mather model [68]:

$$\ln\gamma_i = -\frac{AZ_i^2\sqrt{I}}{1+B\sqrt{I}} + 2\sum_{j\neq w}\beta_{ij}m_j \tag{27}$$

The first and second terms in Eq. (27) are the electrostatic and short-range van der Waals forces. Factors *A* and *B* are determined based on previous studies [65,69], and Z_i (electrical charge) and *I* (ionic strength) are obtained as:

$$I = \frac{1}{2}\sum_i m_j Z_j^2 \tag{28}$$

$$\beta_{ij} = a_{ij} + b_{ij}T \tag{29}$$

where m_j is the concentration of species *j*. β_{ij} in Eq. (27) is the interaction parameter between the molecular species and different ions in the solute–solvent system. Such parameters are set as a function of temperature in Eq. (29).

where a_{ij} and b_{ij} are optimized by the experimental data of CO_2 solubility in DEAB solution [67]. They are tabulated in Table 4.

Table 5
Physicochemical properties used in the Rate-Based model.

Property	Functional dependence	Method	Reference
Liquid phase			
Density	$f(T_L, x_{DEAB})$	Redlich-Kister equation	[73]
Viscosity	$f(T_L, x_{DEAB})$	Redlich-Kister equation	[73]
Surface tension	$f(T_L, x_{DEAB})$		[79]
Heat capacity	$f(T_L, x_{DEAB})$	Redlich-Kister equation	[80]
Henry's constant of CO_2	$f(T_L, x_{DEAB})$	Based on the N_2O analogy	[75]
Diffusivity of CO_2	$f(T_L, x_{DEAB})$	Based on the N_2O analogy	[75]
Diffusivity of DEAB	$f(T_L, x_{DEAB})$	Modified Stokes-Einstein equation	[15]
Heat of reaction of CO_2	$f(P, T_L)$	Gibbs-Helmholtz equation	[12]
Heat of vaporization of H_2O	$f(T_L)$	DIPPR method	[81]
Gas phase			
Density	$f(P, T_G, y_i)$	Peng-Robinson (EOS)	[70]
Viscosity	$f(T_G, y_i)$	Wilke method	[82]
Diffusivity	$f(P, T_G, y_i)$	Fuller equation	[82]
Heat capacity	$f(T_G, y_i)$	DIPPR method	[82]
Thermal conductivity	$f(T_G, y_i)$	Mason and Saxena for mixture,Eucken method for pure compounds	[82]

Along with the above equilibrium constants, the mass-balance relationships are also required:

- Electroneutrality:

$$[DEABH^+] + [H^+] = [HCO_3^-] + [OH^-] + 2[CO_3^{2-}] \quad (30)$$

- Amine balance:

$$[DEAB]_0 = [DEABH^+] + [DEAB] \quad (31)$$

- Carbon balance:

$$\alpha_{CO_2}[DEAB]_0 = [CO_3^{2-}] + [CO_2] + [HCO_3^-] \quad (32)$$

$[DEAB]_0$ is referred to as the preliminary concentration of DEAB. The set of seven nonlinear algebraic equations, i.e., Eqs. (21), (23)–(25), and (30)–(32), are solved using the Newton-Raphson technique to calculate the species concentration at the respective total α_{CO_2} values, such as $[DEAB]$, $[DEABH^+]$, $[CO_2]$, $[HCO_3^-]$, $[CO_3^{2-}]$, $[H^+]$, and $[OH^-]$. In the gas phase, φ_{CO_2} is determined using the Peng − Robinson EOS [70].

2.6. Physicochemical properties

The physicochemical features in the rate-based model are also critical. The physicochemical features for both the liquid and gas phases are provided in Table 5. More details can be found in Appendix A.

2.7. Computational method

Fig. 2 represents the simplified flowchart for the rate-based model of CO_2 capture in a Sulzer DX packed column with DEAB solution. The energy and mass balances, k_G, k_L, and a_e correlations, E models, thermodynamic models, and physicochemical properties were discretized and developed in a MATLAB® script.

A small step size, dZ, is selected to compute the values at each step. First, the compositions of the liquid and gas phases are identified only at the top and bottom of the column. Hence, it becomes a two-point boundary-value problem, which can be solved by the so-called shooting technique in previous studies [29,35,41]. A similar numerical method is initiated at the bottom of the column with the known inlet y_{CO_2} under an initial guess of the outlet condition of DEAB (i.e., L, T_L, and x_{DEAB}). If the α_{CO_2} is more than 0.5 mol CO_2/mol DEAB, Eq. (13) is used to calculate $y_{CO_2,i}$; otherwise, Eq. (14) is used. Finally, after each step is solved by the model, the result of x_{DEAB} at the top segment is compared with the known x_{DEAB} at an inlet.

2.8. Source of experimental data

The CO_2 absorption into DEAB solution was experimentally conducted for a glass packed absorption column (diameter of 0.0275 m and height of 2.15 m) under atmospheric pressure with 37 elements of stainless-steel Sulzer DX type structured packing [43]. The experimental y_{CO_2} and T_L profiles along the column were recorded in a steady-state mode. The experimental conditions and geometric characteristics of the Sulzer DX structured packing are specified in Tables 6 and 7, respectively. The experimental data were used to validate the developed model.

3. Result and discussion

3.1. Sensitivity analysis with mass-transfer correlations

The estimation of E value in a sensitivity analysis with mass-transfer correlations was conducted using the explicit expression [61] for Case 3 in Table 2.

3.1.1. Gas-phase CO_2 mole fraction profiles

A key performance index is the prediction of y_{CO_2} at the absorber outlet. Comparisons between experimental data and simulation results (as typical Runs DX–DE04 and DX–2) are illustrated for each case (A–C) in Fig. 3. y_{CO_2} was reduced with an increase in the packing height of the absorber. The results indicate that the predicted y_{CO_2} using Case A agreed with the experimental data more closely than the other two cases (B and C).

The comparison results for all nine experimental runs are presented in Table 8. The average absolute relative deviation (AARD%) of Case A is 3.12%, whereas those of Cases B and C are 6.75% and 11.63%. Table 8 also illustrates that the highest deviation in y_{CO_2} between the experimental data, and simulated results in Cases A and B were observed in Runs DX-DE02, DX-DE04, and DX-DE05, where T_L is higher than 30 °C. For Case C, the DEAB concentration (C_{DEAB}) was less than 2 kmol/m^3. Fig. 4. depicts the capability of the three cases in the prediction of the experimental data. The correlation coefficient (R^2) values indicate that the accuracy of Case A ($R^2 = 0.9889$) is higher than that of Cases B ($R^2 = 0.9834$) and C ($R^2 = 0.9682$) in predicting y_{CO_2}.

3.1.2. Temperature profiles

By absorbing CO_2 with the DEAB solution, the reactions release heat to the solution. A part of the heat evolved from the rich DEAB is taken up by the flue gas at the absorber bottom. Therefore, the temperature of the flue gas stream increases from the bottom up to near the top of the absorber, in which heating the lean DEAB occurs through contact with the up-flowing flue gas. As the reaction heats, H_2O is vaporized and then condensed by the colder lean-DEAB while it rises along the absorber.

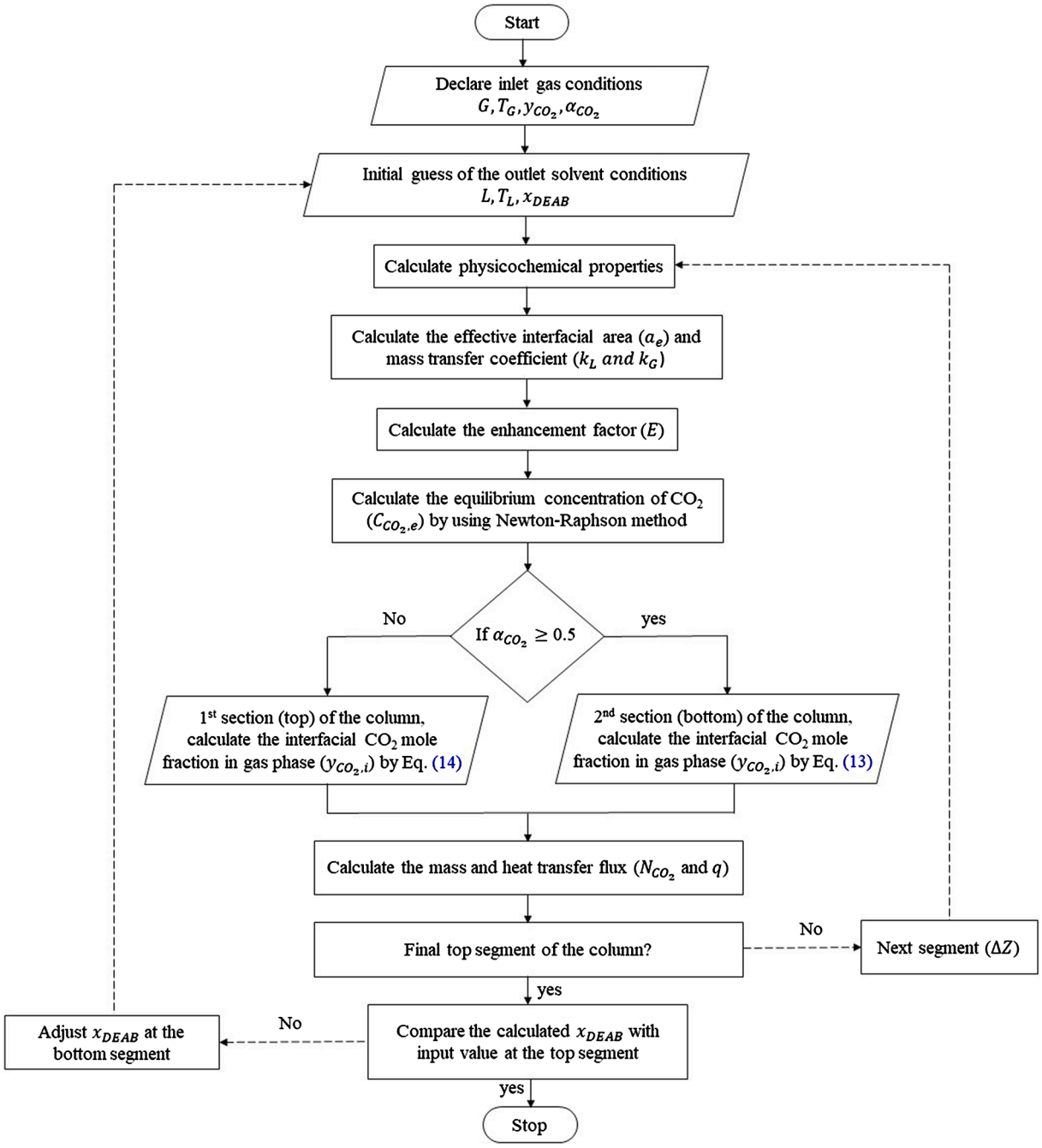

Fig. 2. Computational flowchart of Rate-Based model for CO_2 absorption using DEAB solution in a Sulzer DX packed column.

Table 6
Experimental conditions for the CO_2 absorption using DEAB solution in a Sulzer DX packed column [43].

Description	DX-DE01	DX-DE02	DX-DE03	DX-DE04	DX-DE05	DX-1a	DX-2	DX-1b	DX-1c
Gas flow rate (L/min)	4.5	4.5	4.5	4.5	4.5	4.5	4.5	4.5	4.5
Gas inlet temperature (°C)	24.0	26.0	23.8	24.4	25.1	24.6	25.5	26	24.7
Gas phase CO_2 concentration (mol%)	14.6	14.6	14.4	14.4	14.4	14.6	14.6	14.6	14.6
CO_2 removal efficiency (%)	68.8	71.3	60.4	66.9	79.7	62.1	64.1	68.5	67.3
Liquid flow rate (mL/min)	50	50	50	50	50	40	50	50	74
Liquid inlet temperature (°C)	22.8	30.1	23.3	30.5	39.3	23	23.2	23.2	23.1
Amine concentration (kmol/m^3)	2.0	1.6	1.1	1.1	1.1	2.0	2.0	2.0	2.0
Inlet CO_2 loading (mol CO_2/mole amine)	0.1	0.1	0.2	0.2	02	0.3	0.3	0.1	0.1
Outlet CO_2 loading (mol CO_2/mole amine)	0.3	0.4	0.7	0.7	0.7	0.5	0.4	0.3	0.3
Pressure (kPa)	102.0	102.0	101.7	101.7	101.7	101.4	101.4	101	101.2

Table 7
Characteristics of Sulzer DX structured packing.

Parameters	Specifications
Material packing	Stainless steel
Surface area,a	900 (m^2/m^3)
Void fraction,ε	0.775 (m^3/m^3)
Crimp angle,θ	60°
Corrugation height, h	2.9 mm

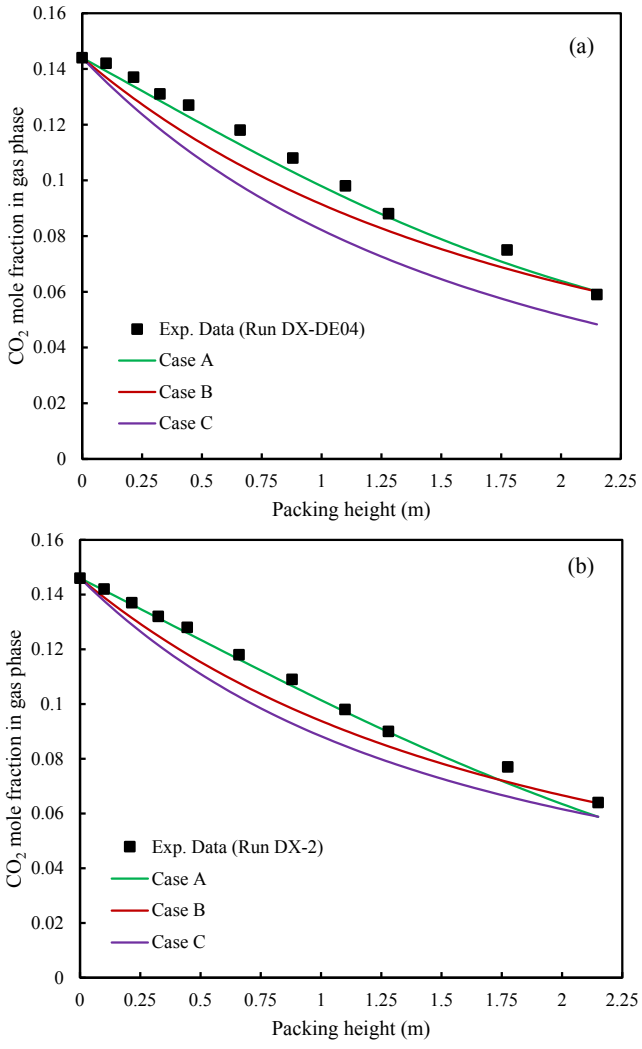

Fig. 3. Sensitivity analysis of y_{CO_2} profiles along the Sulzer DX packed column using different cases of k_G, k_L and a_e correlations: (a) Run DX–DE04 and (b) Run DX–2.

Thus, a considerable temperature bulge can be observed in the T_L and T_G profiles of the absorber (Fig. 5).

The location of the bulge is predominantly based on the L/G ratio and the heat capacity of liquid [71]. However, the bulge's increased magnitude also resulted from a higher heat of absorption and alteration in the gas-phase CO_2 concentration. Therefore, it is vital to select an appropriate mass-transfer correlation to obtain precise outcomes from the rate-based model. At this point, the sensitivity of T_L and T_G profiles along the Sulzer DX packed column were assessed using Cases A to C.

Fig. 5. illustrates the comparison between the experimental data and the predicted T_L and T_G profiles under the operating circumstances of Runs DX–DE03 and DX–1a in Table 6. The difference between T_L and T_G at the column bottom indicated an exothermic reaction between CO_2 and DEAB solution, resulting from an increment in T_L and T_G at the column bottom.

The parabolic profiles of T_L and T_G indicated that CO_2 was captured thoroughly by all cases (A, B, and C) because the L/G ratio of experimental runs is high. However, the predicted convex magnitudes of Cases B and C are less than that of Case A. This result implies that Case A is more reasonable than the other two cases. The AARD% of the predicted T_L value by comparing with all nine experimental runs is listed in Table 8 to confirm the results. The results are consistent that Case A (AARD%=2.09) offers less error than Cases B (AARD%=2.43) and C (AARD%=2.77) in the prediction of T_L. Fig. 6. illustrates the parity plots of the calculated data against the experimental data for T_L obtained by Cases A to C. The R^2 values indicate that Case A ($R^2 = 0.9685$) has higher accuracy in the estimation of the experimental data than the other two cases (Cases B ($R^2 = 0.9458$) and C ($R^2 = 0.9395$)).

3.1.3. CO_2 loading profiles

Because C_{DEAB} has a significant effect on the α_{CO_2} profile, decreasing the concentration led to increasing α_{CO_2} and reducing the cost of regeneration [16]. The regeneration predominantly affects the capital cost of gas treating plants[63].

Fig. 7. illustrates the α_{CO_2} profiles of DEAB solution along the Sulzer DX packed column using different cases (A to C in Table 1) whose operating conditions are presented in Table 6. The operating results of α_{CO_2} from the pilot plant were measured only at the top and bottom of the Sulzer DX packed column [43]. Cases A and B could accurately predict the top outlet α_{CO_2} for Runs DX-DE05 and DX-1b, but the trend in α_{CO_2} changing along the column is different. It is challening to conclude which is the more accurate profile of α_{CO_2}; nevertheless, the slope of the α_{CO_2} profile along the column is similar to that of the y_{CO_2} profile. As described in Section 3.1.1, considering the prediction accuracy of the y_{CO_2} profile in Case A compared with the other cases, Case A would be more accurate in predicting the α_{CO_2} profile.

3.1.4. Gas-phase H_2O mole fraction

Fig. 8. illustrates the y_{H_2O} profiles along the Sulzer DX packed column for the different Cases A to C. Due to the highest heat release from the reaction between DEAB solution and CO_2 at the column bottom, H_2O can be evaporated and rises. By flowing up the gas along the column, the cold DEAB solution condenses the H_2O at the top of the column. Therefore, due to the higher T_L entering the column in Run DX-DE05 (Fig. 8a), the amount of evaporated H_2O is higher than in Run DX-1c (Fig. 8b). Because the H_2O vapor pressure equation is a function of T_L and the k_G, k_L and a_e of Case A exhibit the optimal outcomes for T_L profiles compared with the other cases (Section 3.1.2). Consequently, Case A might predict reasonably the y_{H_2O} profile.

3.2. Sensitivity analysis with enhancement factor correlations

After choosing Case A as the most accurate correlation of k_G, k_L and a_e in the sensitivity analysis (Section 3.1), the effects of five different E correlations, introduced in Section 2.4, on the rate-based model were investigated. The E value is a crucial parameter for chemical absorption and must be accurately estimated for appropriate modeling of mass transfer. Several aspects affect E, including the physical features of gas and liquid, the gas-phase CO_2 concentration, the amine concentration in the liquid phase, the reaction rate, and the flow field [72].

Figs. 9–11 illustrate the effects of α_{CO_2}, T_L, and L on the calculated E values, respectively. The convex shape at the column bottom in these figures is caused by the higher reaction rate between DEAB solution and CO_2 at the bottom than at the top of the column.

Fig. 9. illustrates the results for Runs DX-DE01, DX-2, and DX-DE03, where α_{CO_2} values at the column bottom are 0.3, 0.4, and 0.7 mol CO_2/mol DEAB. Based on the results, when the α_{CO_2} of the rich DEAB solution increases to 0.4 (Run DX-2) and 0.7 (Run DX-DE03) mol CO2/mol

Table 8
Average absolute relative deviation (AARD%) between calculated and experimental data of mole fraction of CO_2 in gas phase (y_{CO_2}) and liquid phase temperature (T_L).[a]

Runs	DX-DE01	DX-DE02	DX-DE03	DX-DE04	DX-DE05	DX-1a	DX-2	DX-1b	DX-1c	
	mole fraction of CO_2 in gas phase									AARD%
Case A	2.76	3.39	2.58	3.45	5.75	2.40	2.54	2.54	2.72	3.12
Case B	5.73	7.46	6.06	7.37	10.65	6.18	5.91	5.31	6.24	6.75
Case C	10.04	11.27	12.23	15.20	17.22	10.07	10.34	9.32	9.66	11.63
	Liquid-phase temperature									
Case A	2.16	2.22	2.56	2.40	2.24	1.72	1.81	1.72	2.00	2.09
Case B	2.13	2.62	3.53	2.64	2.62	2.57	1.94	1.41	2.45	2.43
Case C	2.39	2.60	3.30	3.20	3.84	2.77	2.49	1.93	2.38	2.77

[a] $AARD\% = \frac{1}{N}\sum_{i=1}^{n}\frac{\left|Y_i^{Cal} - Y_i^{Exp}\right|}{Y_i^{Exp}} = \frac{1}{N}\sum_{i=1}^{n}(ARD\%)_i$.

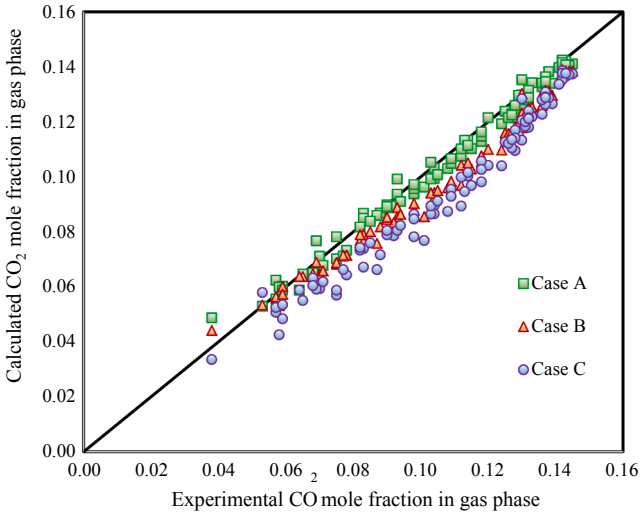

Fig. 4. Parity plot of calculated and experimental y_{CO_2} along the Sulzer DX packed column using different cases of k_G, k_L and a_e correlations for all runs.

DEAB, the E values decrease considerably due to the consumption of the reactive species with loading. The concentration decrease in the input DEAB reduces the reaction rate and E value. Hence, in Run DX-DE03, the slope of the E profile at the top section of the column increases compared with the Runs DX-DE01 and DX-2 due to a decrease in the concentration of the input DEAB (1.1 kmol/m^3).

Fig. 10. represents the effects of T_L on the E values under the operating conditions of Runs DX-DE03, DX-DE04, and DX-DE05, where the T_L values at the top of the column are 23.3, 30.5, and 39.3 °C. According to the Arrhenius equation, because the increment in T_L mostly results in a higher reaction rate between amine solution and CO_2, the mass-transfer and CO_2 removal efficiency are improved. Fig. 10. reveals that increasing T_L at the inlet is caused by decreasing E value at the bottom section of the column. The magnitude and position of the E bulge slightly increases. Finally, the slop of the E value at the top section of the absorber decreases. Hence, the reaction rate and resultant CO_2 removal efficiency are higher in Run DX-DE05 (79.7%) than in Runs DX-DE04 (66.9%) and DX-DE03 (60.4%).

The effects of L on E values under the operating conditions of Runs DX-1b and DX-1c, where L values are 50 and 74 ml/min, are presented in Fig. 11. This factor is vital to the absorber because increasing the amine flow rate increases the free-amine molecules for higher CO_2 removal. Therefore, it enhances the CO_2 removal efficiency by reducing the mass-transfer resistance in the liquid phase and increases the a_e of the packing by closely contacting amine with gas in the column.

Nevertheless, by increasing more than the optimal circumstances, the CO_2 removal efficiency can be deteriorated by flooding in the absorption column. This behavior is observed in Fig. 11; with the increasing L, the value of E at the column bottom does not change, and

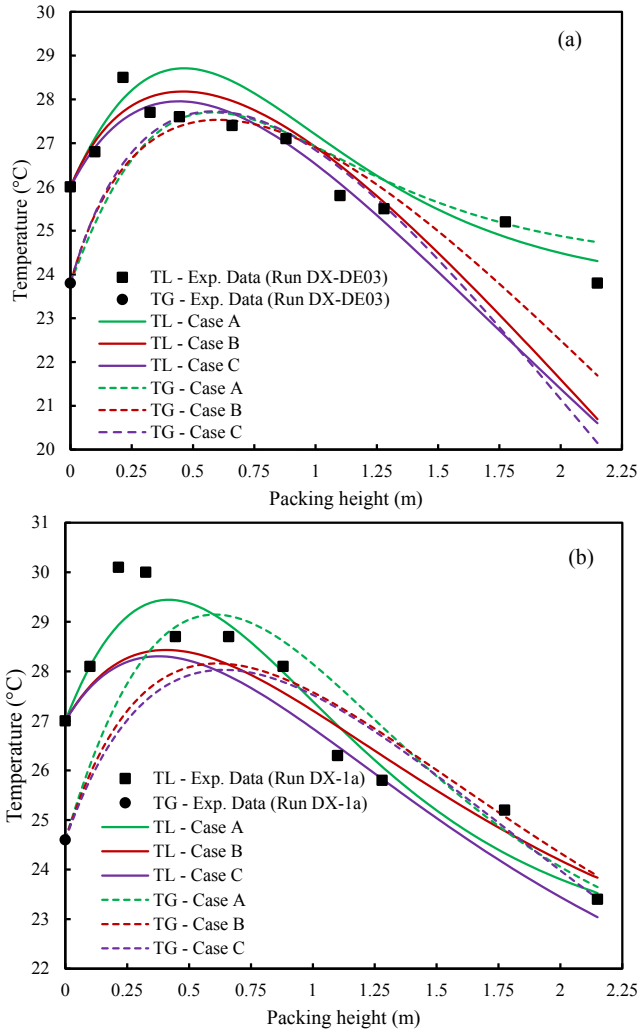

Fig. 5. Sensitivity analysis of $T_L$and T_G profiles along the Sulzer DX packed column using different cases of k_G, k_L and $a_e$correlations: (a) Run DX–DE03 and (b) Run DX–1a.

the magnitude of the bulge decreases, whereas the slop of E value at the column top decreases. Therefore, because the reaction rate increases at the column top, it is expected that the CO_2 removal efficiency can increase in the Run DX-1c (67.3%) compared with the Run DX-1b run (68.5%). However, due to the increase above the optimal value of L, it decreased.

Figs. 9–11 also illustrate the plots of the obtained E values from the five E correlations tested. The results from all the Runs reveal that the E values obtained from Case 3 overlap with Case 4, and Cases 1 and 5 are close together and yield slightly higher E values than Cases 3 and 4.

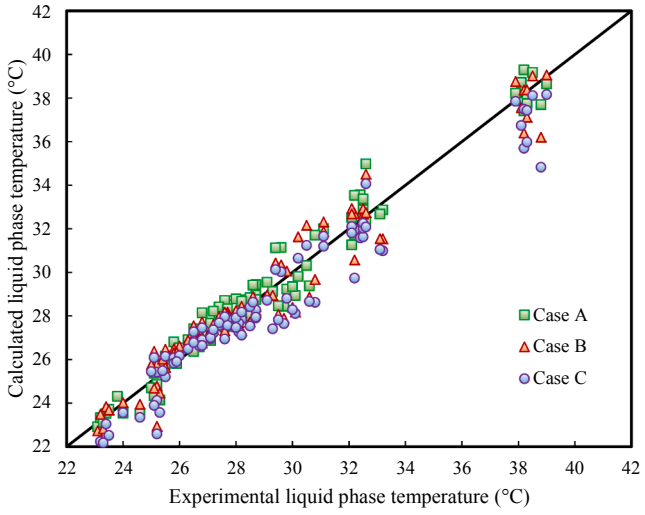

Fig. 6. Parity plot of calculated and experimental T_L along the Sulzer DX packed column using different cases of k_G, k_L and a_e correlations for all runs.

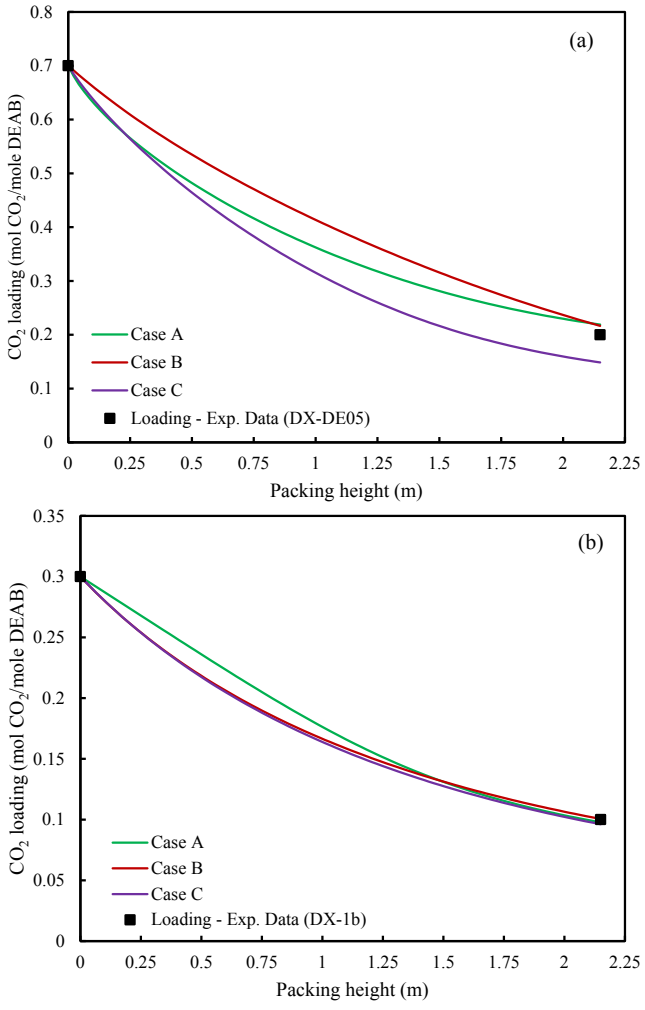

Fig. 7. Sensitivity analysis of α_{CO_2} profiles along the Sulzer DX packed column using different cases of k_G, k_L and $a_e$correlations: (a) Run DX-DE05 and (b) Run DX-1b.

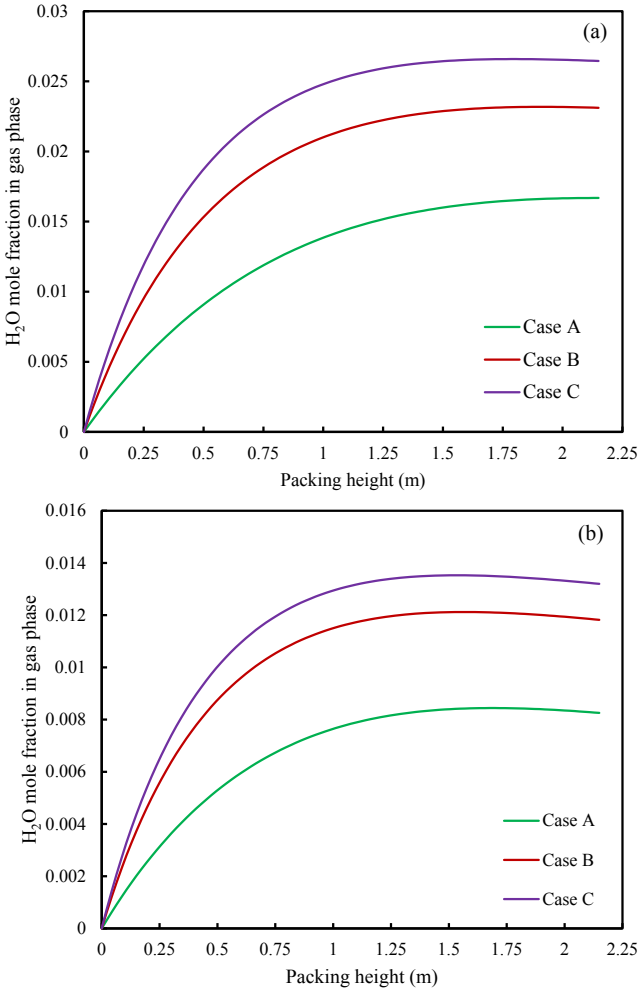

Fig. 8. Sensitivity analysis of y_{H_2O} profiles along the Sulzer DX packed column using different cases of k_G, k_L and $a_e$correlations: (a) Run DX-DE05 and (b) Run DX-1c.

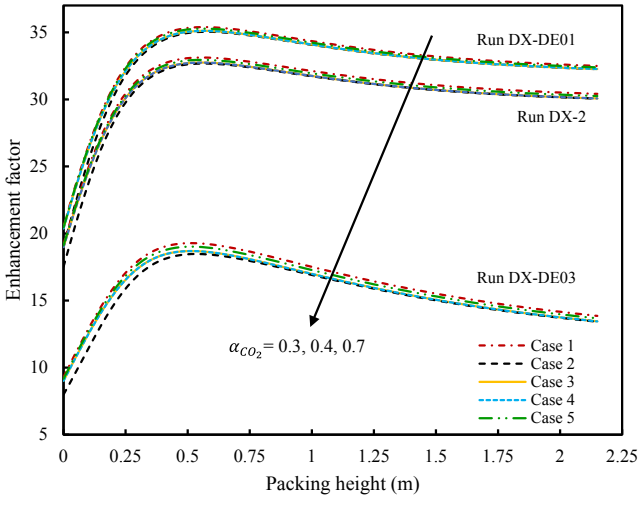

Fig. 9. Effect of α_{CO_2} on the E values along the Sulzer DX packed column. (–·–) Case 1, (– – –) Case 2, (—) Case 3, (- - -) Case 4, and (–··–) Case 5.

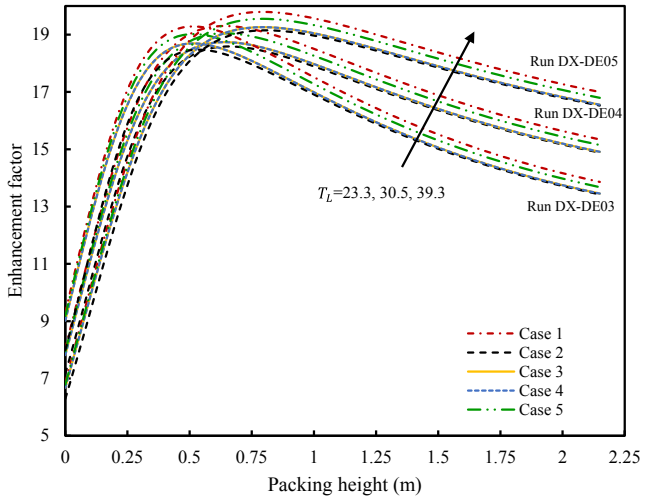

Fig. 10. Effect of T_L on the E values along the Sulzer DX packed column. (– • –) Case 1, (– – –) Case 2, (—) Case 3, (- - -) Case 4, and (– • • –) Case 5.

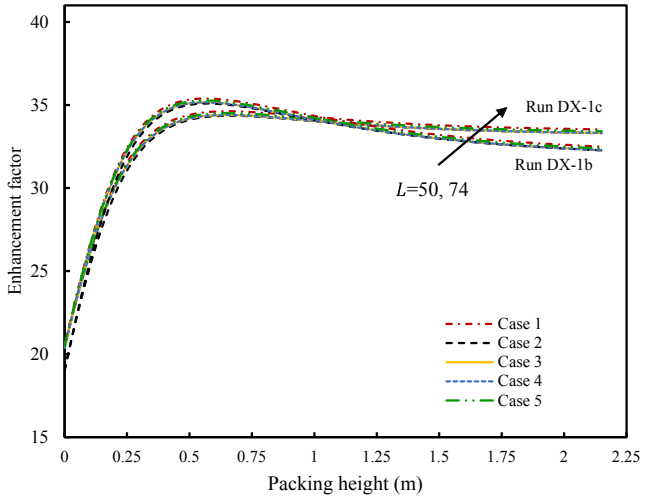

Fig. 11. Effect of L on the E values along the Sulzer DX packed column. (– • –) Case 1, (– – –) Case 2, (—) Case 3, (- - -) Case 4, and (– • • –) Case 5.

Moreover, Case 2 exhibits a deviation at the low packing height (<0.5 m).

In Fig. 9, the former conditions were observed in Runs DX-DE01, DX-2, and DX-DE03, with the difference that the discrepancies between the calculated E values by different correlations become more distinct when increasing α_{CO_2} from 0.3 (Run DX-DE01) to 0.7 (Run DX-DE03) mol CO_2/mol DEAB. In contrast, in Figs. 10 and 11 for all the Runs, the discrepancies between the calculated E values by different correlations remained constant with the change of T_L and L. The discrepancies between the obtained E values by five E correlations are practically related to α_{CO_2} and independent T_L and L. The E relationships used in this study do not significantly affect the calculated E values because similar values are obtained from all the relationships.

4. Conclusion

The absorption of CO_2 into DEAB solution in a Sulzer DX packed column was investigated by developing a rate-based model. For increased model accuracy, especially at high α_{CO_2}, and simplified model calculations, the absorber was divided into two sections: in α_{CO_2}, less than 0.5 mol CO_2/mol DEAB and more than 0.5 mol CO_2/mol DEAB. At α_{CO_2} of less than 0.5, the $C_{CO_{2,e}}$ was neglected, while, at higher α_{CO_2}, the Deshmukh – Mather activity coefficient model was used to calculate $C_{CO_{2,e}}$. Then, the validation and sensitivity analysis were performed using different k_G, k_L, and a_e correlations for the prediction of α_{CO_2}, y_{H_2O}, y_{CO_2}, T_L, and T_G profiles along the Sulzer DX packed column. The findings indicate that the developed rate-based model in Case A (i.e., k_G and k_L and a_e) produced AARD% = 3.12 and R^2 = 0.9889 for y_{CO_2} and AARD % = 2.09 and R^2 = 0.9685 for T_L, which are higher than in Cases B and C. This result is likely because k_G and k_L were used in the case of tertiary amines such as DEAB and a_e was designed specifically for Sulzer DX packing.

The effects of α_{CO_2}, T_L, and L as the most critical parameters of absorber on the E value were investigated. The results confirmed that α_{CO_2} has a significant impact on the E values and consequently on the reaction rate. Finally, the sensitivity analysis of E correlations at the same condition confirms that the various E relationships used generally produce the same E values. The results in this study highlight the prospect of future process development and optimization for efficient CO_2 capture.

CRediT authorship contribution statement

Peyman Pakzad: Conceptualization, Methodology, Investigation, Data curation, Software, Writing - original draft. **Masoud Mofarahi:** Validation, Visualization, Supervision, Writing - review & editing, Funding acquisition. **Chang-Ha Lee:** Supervision, Writing - review & editing, Funding acquisition.

Declaration of Competing Interest

The authors declare that they have no known competing financial interests or personal relationships that could have appeared to influence the work reported in this paper.

Acknowledgments

The authors are sincerely grateful for the sponsorships from the Persian Gulf University and Yonsei University. This work was supported by the National Research Foundation of Korea (NRF), funded by the Ministry of Science and ICT (2019K1A4A7A03113187).

Appendix A. . Physicochemical properties

Density and viscosity of DEAB solution

The density and viscosity of DEAB solution (ρ_L;gr/cm^3 and μ_L; g/cm.s) is determined using the Redlich-Kister equation developed by Maneeintr et al. [73]:

$$P_L = \Delta P + x_1 P_1 + x_2 P_2 \quad \text{(A1)}$$

$$\Delta P = x_1 x_2 \sum_{i=0}^{n} A_i (x_1 - x_2)^i \quad \text{(A2)}$$

Table A1
Values of the interaction parameters (A_i) corresponding to the Redlich–Kister equation of excess molar volume (V^E) of DEAB solution [73].

$T(K)$	A_0	A_1	A_2	A_3	A_4
298.15	−8.5521	2.8880	3.1626	6.2376	−3.8402
303.15	−8.3403	2.8631	3.1617	6.0730	−3.5970
313.15	−8.1808	2.5692	5.3194	6.3602	−5.8303
323.15	−7.7258	2.2818	6.4097	7.3950	−8.6067
333.15	−7.2046	1.5802	6.8354	12.893	−15.395
343.15	−6.9566	3.4085	16.292	−30.437	21.665

Table A2
Values of the interaction parameters (A_i) corresponding to the Redlich–Kister equation of viscosity deviation ($\Delta\eta$) of DEAB solution [73].

$T(K)$	A_0	A_1	A_2	A_3	A_4
298.15	38.10	−73.90	55.70	51.70	−76.30
303.15	28.00	−52.50	39.40	32.70	−49.50
313.15	15.60	−23.70	19.40	5.07	−14.70
323.15	9.61	−12.8	10.80	−4.60	−1.22
333.15	6.33	−8.31	5.58	−4.02	2.86
343.15	4.30	−6.38	3.06	6.77	−7.50

Table A3
Values of the adjustable parameters ($a_{i,0}$ and $a_{i,1}$) corresponding to the Redlich–Kister equation of excess molar heat capacity (C_P^E) of DEAB solution [74]

Interaction parameters	Adjustable parameters	
	$a_{1,0}$	$a_{1,1}$
A_1	0.99649	−0.04858
	$a_{2,0}$	$a_{2,1}$
A_2	0.99656	−0.0234

where P_L represents ρ_L or μ_L, ΔP refers to excess molar volume (V^E) and viscosity deviation ($\Delta\eta$), P and x with subscripts 1 and 2 denote pure density or viscosity and mole fraction of DEAB and H_2O, respectively. n is the degree of the polynomial, A_i represents the interaction parameters provided in Tables A1 and A2 for density and viscosity.

Heat capacity of DEAB solution

Pouryousefi Dargah [74] measured the molar heat capacity ($C_{p,L}$; J/mol.K) of DEAB solution and correlated the data with the Redlich-Kister equation as follows:

$$C_{p,L} = C_P^E + x_1 C_{p,1} + x_2 C_{p,2} \tag{A3}$$

$$C_P^E = x_1 x_2 \sum_{i=1}^{n} A_i (x_1 - x_2)^{i-1} \tag{A4}$$

where C_P^E is the excess molar heat capacity of the solution and C_p and x with subscripts 1 and 2 are the pure heat capacity and mole fraction of DEAB and H_2O. A_i is the interaction parameter as a function of temperature based on the following equation:

$$A_i = a_{i,0} + a_{i,1}(T) \tag{A5}$$

where a_i and b_i are adjustable parameters whose values are presented in Table A3.Henry's constant of CO_2 in DEAB solution.

Henry's constant of CO_2 in DEAB solution (H_{CO2}; kPa.m^3/K.mol) in Eqs. (13) and (14) was calculated by the nitrous oxide (N_2O) analogy as follows:

$$H_{CO_2} = H_{N_2O-DEAB}\left(\frac{H_{CO_2-H_2O}}{H_{N_2O-H_2O}}\right) \tag{A6}$$

Henry's constant of N_2O in pure DEAB ($H_{N_2O-DEAB}$) is determined from an exponential function with temperature, developed by Sema et al. [75].

$$H_{N_2O-DEAB} = 1.1876 \times 10^7 \exp\left(\frac{-2460.3}{T}\right) \tag{A7}$$

Henry's constant of CO_2 and N_2O in H_2O ($H_{CO_2-H_2O}$ and $H_{N_2O-H_2O}$) in Eq. (A6) can be obtained in kPa m^3/K mol from the correlations presented by Versteeg and van Swaaij [76] as

$$H_{CO_2-H_2O} = 2.82 \times 10^6 \exp\left(\frac{-2044}{T}\right) \tag{A8}$$

$$H_{N_2O-H_2O} = 8.55 \times 10^6 \exp\left(\frac{-2284}{T}\right) \tag{A9}$$

$$D_{CO_2,L} = D_{N_2O-DEAB}\left(\frac{D_{CO_2-H_2O}}{D_{N_2O-H_2O}}\right)^{0.8} \quad \text{A10)}$$

Diffusivity of CO_2 in the liquid phase

Due to the chemical reaction of CO_2 with DEAB, the CO_2 diffusivity in the DEAB solution ($D_{CO_2,L}$; m^2/s) is also determined from the N_2O analogy, where $D_{CO_2-H_2O}$ and $D_{N_2O-H_2O}$ are the CO_2 and N_2O diffusivities in water in m^2/s and $D_{N_2O-DEAB}$ is the diffusivity of N_2O in DEAB solution in m^2/s. $D_{CO_2-H_2O}$ and $D_{N_2O-H_2O}$ are calculated from the correlations of Versteeg and van Swaaij [76],

$$D_{CO_2-H_2O} = 2.35 \times 10^{-6}\exp(\frac{-2119}{T}) \quad \text{(A11)}$$

$$D_{N_2O-H_2O} = 5.07 \times 10^{-6}\exp(\frac{-2371}{T}) \quad \text{(A12)}$$

$D_{N_2O-DEAB}$ is determined from a semi-empirical model with temperature and DEAB concentration (C_{DEAB}; mol/L) in cm^2/s, developed by Sema et al. [75],

$$D_{N_2O-DEAB} = \left(4.64 \times 10^{-8} + 8.74 \times 10^{-8}C_{DEAB} + 2.86 \times 10^{-8}C_{DEAB}^2\right)\exp\left(\frac{-9.5 - 3.81C_{DEAB}}{T}\right) \quad \text{(A13)}$$

Diffusivity of the DEAB in the liquid phase

The diffusivity of DEAB in DEAB solution ($D_{DEAB,L}$;cm^2/s) is determined using the modified Stokes-Einstein correlation developed by Sema et al. [15],

$$D_{DEAB,L} = \left(1.739 \times 10^{-9}\right)\mu_L^{-0.569842}T \quad \text{(A14)}$$

where μ_L is the viscosity of DEAB solution in g/cm s, which was calculated in Section A.1 of Appendix A.

References

[1] Climate Change 2014: Synthesis Report. Contribution of Working Groups I, II and III to the Fifth Assessment Report of the Intergovernmental Panel on Climate Change; IPCC: Geneva, Switzerland, (2014)., n.d.

[2] D. Pandey, M.K. Mondal, Equilibrium CO_2 solubility in the aqueous mixture of MAE and AEEA: experimental study and development of modified thermodynamic model, Fluid Phase Equilib. 522 (2020), 112766.

[3] D.Q. Gbadago, H.-T. Oh, D.-H. Oh, C.-H. Lee, M. Oh, CFD simulation of a packed bed industrial absorber with interbed liquid distributors, Int. J. Greenh. Gas Control. 95 (2020), 102983.

[4] H.-T. Oh, Y. Ju, K. Chung, C.-H. Lee, Techno-economic analysis of advanced stripper configurations for post-combustion CO_2 capture amine processes, Energy. 206 (2020), 118164.

[5] S.-Y. Oh, S. Yun, J.-K. Kim, Process integration and design for maximizing energy efficiency of a coal-fired power plant integrated with amine-based CO_2 capture process, Appl. Energy. 216 (2018) 311–322.

[6] W.-S. Lee, J.-H. Kang, J.-C. Lee, C.-H. Lee, Enhancement of energy efficiency by exhaust gas recirculation with oxygen-rich combustion in a natural gas combined cycle with a carbon capture process, Energy. 117586 (2020).

[7] K.M.S. Salvinder, H. Zabiri, S.A. Taqvi, M. Ramasamy, F. Isa, N.E.M. Rozali, H. Suleman, A. Maulud, A.M. Shariff, An overview on control strategies for CO_2 capture using absorption/stripping system, Chem. Eng. Res. Des. 147 (2019) 319–337.

[8] B.K. Mondal, S.S. Bandyopadhyay, A.N. Samanta, Equilibrium solubility and enthalpy of CO_2 absorption in aqueous bis (3-aminopropyl) amine and its mixture with MEA, MDEA, AMP and K_2CO_3, Chem. Eng. Sci. 170 (2017) 58–67.

[9] Y. Wu, J. Xu, K. Mumford, G.W. Stevens, W. Fei, Y. Wang, Recent advances in carbon dioxide capture and utilization with amines and ionic liquids, Green Chem. Eng. (2020).

[10] F.A. Chowdhury, H. Yamada, T. Higashii, K. Goto, M. Onoda, CO_2 capture by tertiary amine absorbents: a performance comparison study, Ind. Eng. Chem. Res. 52 (2013) 8323–8331.

[11] P. Tontiwachwuthikul, A.G.H. Wee, R. Idem, K. Maneeintr, G. Fan, A. Veawab, A. Henni, A. Aroonwilas, A. Chakma, Method of capturing carbon dioxide from gas streams, (2011).

[12] T. Sema, A. Naami, R. Idem, P. Tontiwachwuthikul, Correlations for equilibrium solubility of carbon dioxide in aqueous 4-(diethylamino)-2-butanol solutions, Ind. Eng. Chem. Res. 50 (2011) 14008–14015.

[13] M. Afkhamipour, M. Mofarahi, Modeling and optimization of CO_2 capture using 4-diethylamino-2-butanol (DEAB) solution, Int. J. Greenh. Gas Control. 49 (2016) 24–33.

[14] K. Maneeintr, R.O. Idem, P. Tontiwachwuthikul, A.G.H. Wee, Synthesis, solubilities, and cyclic capacities of amino alcohols for CO_2 capture from flue gas streams, Energy Procedia. 1 (2009) 1327–1334.

[15] T. Sema, A. Naami, K. Fu, G. Chen, Z. Liang, R. Idem, P. Tontiwachwuthikul, Comprehensive mass transfer and reaction kinetics studies of a novel reactive 4-diethylamino-2-butanol solvent for capturing CO_2, Chem. Eng. Sci. 100 (2013) 183–194.

[16] A. Naami, M. Edali, T. Sema, R. Idem, P. Tontiwachwuthikul, Mass transfer performance of CO_2 absorption into aqueous solutions of 4-diethylamino-2-butanol, monoethanolamine, and N-methyldiethanolamine, Ind. Eng. Chem. Res. 51 (2012) 6470–6479.

[17] J. Xue, Q. Li, J. Qi, Q. Wu, H. Zhao, L. Zhang, Multi-scale study of wet pressure drop model for a novel structured wire gauze packing, Chem. Eng. Sci. 230 (n.d.) 116179.

[18] A. Ghaemi, A. Hemmati, Mass transfer coefficient for PZ+ CO_2+ H_2O system in a packed column, Heat Mass Transf. 1–15 (2020).

[19] H. Ling, H. Gao, Z. Liang, Comprehensive solubility of N_2O and mass transfer studies on an effective reactive N, N-dimethylethanolamine (DMEA) solvent for post-combustion CO_2 capture, Chem. Eng. J. 355 (2019) 369–379.

[20] J. Liu, S. Wang, G. Qi, B. Zhao, C. Chen, Kinetics and mass transfer of carbon dioxide absorption into aqueous ammonia, Energy Procedia. 4 (2011) 525–532.

[21] H. Gao, S. Liu, X. Luo, H. Zhang, Z. Liang, Investigation of hydrodynamic performance and effective mass transfer area for Sulzer DX structured packing, AIChE J. 64 (2018) 3625–3637.

[22] H. Liao, H. Gao, B. Xu, Z. Liang, Mass transfer performance studies of aqueous blended DEEA-MEA solution using orthogonal array design in a packed column, Sep. Purif. Technol. 183 (2017) 117–126.

[23] M. Llano-Restrepo, E. Araujo-Lopez, Modeling and simulation of packed-bed absorbers for post-combustion capture of carbon dioxide by reactive absorption in aqueous monoethanolamine solutions, Int. J. Greenh. Gas Control. 42 (2015) 258–287.

[24] S. Moioli, L.A. Pellegrini, Regeneration section of CO_2 capture plant by MEA scrubbing with a rate-based model, Chem. Eng. Trans. 32 (2013) 1849–1854.

[25] C.V. Brand, E. Graham, J. Rodriguez, A. Galindo, G. Jackson, C.S. Adjiman, On the use of molecular-based thermodynamic models to assess the performance of solvents for CO_2 capture processes: monoethanolamine solutions, Faraday Discuss. 192 (2016) 337–390.

[26] M. Afkhamipour, M. Mofarahi, Comparison of rate-based and equilibrium-stage models of a packed column for post-combustion CO_2 capture using 2-amino-2-methyl-1-propanol (AMP) solution, Int. J. Greenh. Gas Control. 15 (2013) 186–199.

[27] A. Lawal, M. Wang, P. Stephenson, H. Yeung, Dynamic modelling of CO_2 absorption for post combustion capture in coal-fired power plants, Fuel. 88 (2009) 2455–2462.

[28] F.M. Khan, V. Krishnamoorthi, T. Mahmud, Modelling reactive absorption of CO_2 in packed columns for post-combustion carbon capture applications, Chem. Eng. Res. Des. 89 (2011) 1600–1608.

[29] N.A.H. Hairul, A.M. Shariff, W.H. Tay, Ama. Mortel, K.K. Lau, L.S. Tan, Modelling of high pressure CO2 absorption using PZ+AMP blended solution in a packed absorption column, Sep. Purif. Technol. 165 (2016) 179–189.

[30] G.Q. Wang, X.G. Yuan, K.T. Yu, Review of mass-transfer correlations for packed columns, Ind. Eng. Chem. Res. 44 (2005) 8715–8729.

[31] A. Hemmati, H. Rashidi, Mass transfer investigation and operational sensitivity analysis of amine-based industrial CO_2 capture plant, Chinese J. Chem. Eng. 27 (2019) 534–543.

[32] M. Afkhamipour, M. Mofarahi, Sensitivity analysis of the rate-based CO_2 absorber model using amine solutions (MEA, MDEA and AMP) in packed columns, Int. J. Greenh. Gas Control. 25 (2014) 9–22.

[33] R.L. Kent, B. Eisenberg, Better data for amine treating, Hydrocarb. Process. 55 (1976) 87–90.

[34] J. Gabrielsen, M.L. Michelsen, E.H. Stenby, G.M. Kontogeorgis, A model for estimating CO_2 solubility in aqueous alkanolamines, Ind. Eng. Chem. Res. 44 (2005) 3348–3354.

[35] M.Z. Shahid, A.S. Maulud, M.A. Bustam, H. Suleman, H.N.A. Halim, A.M. Shariff, Rate-based modeling for packed absorption column of the MEA-CO_2-water system at high-pressure and high-CO_2 loading conditions, Ind. Eng. Chem. Res. 58 (2019) 12235–12246.

[36] A.T. Zoghi, F. Feyzi, M.R. Dehghani, Modeling CO_2 solubility in aqueous N-methyldiethanolamine solution by electrolyte modified Peng-Robinson plus association equation of state, Ind. Eng. Chem. Res. 51 (2012) 9875–9885.

[37] R.D. Deshmukh, A.E. Mather, A mathematical model for equilibrium solubility of hydrogen sulfide and carbon dioxide in aqueous alkanolamine solutions, Chem. Eng. Sci. 36 (1981) 355–362.

[38] D.M. Austgen, G.T. Rochelle, X. Peng, C.C. Chen, Model of vapor-liquid equilibria for aqueous acid gas-alkanolamine systems using the electrolyte-NRTL equation, Ind. Eng. Chem. Res. 28 (1989) 1060–1073.

[39] M.L. Posey, G.T. Rochelle, A thermodynamic model of methyldiethanolamine-CO_2-H_2S-water, Ind. Eng. Chem. Res. 36 (1997) 3944–3953.

[40] H. Suleman, A.S. Maulud, Z. Man, Review and selection criteria of classical thermodynamic models for acid gas absorption in aqueous alkanolamines, Rev. Chem. Eng. 31 (2015) 599–639.

[41] M. Afkhamipour, M. Mofarahi, Rate-based modeling and sensitivity analysis of a packed column for post-combustion CO_2 capture into a novel reactive 1-dimethylamino-2-propanol (1DMA2P) solution, Int. J. Greenh. Gas Control. 65 (2017) 137–148.

[42] F.A. Tobiesen, H.F. Svendsen, O. Juliussen, Experimental validation of a rigorous absorber model for CO_2 postcombustion capture, AIChE J. 53 (2007) 846–865.

[43] A. Naami, Mass transfer studies of carbon dioxide absorption into aqueous solutions of 4-(diethylamine)-2-butanol, blended monoethanolamine with 4-(diethylamine)-2-butanol, and blended monoethanolamine with methyldiethanolamine, Faculty of Graduate Studies and Research, University of Regina, 2013.

[44] J.D. Pandya, Adiabatic gas absorption and stripping with chemical reaction in packed towers, Chem. Eng. Commun. 19 (1983) 343–361.

[45] T.H. Chilton, A.P. Colburn, Mass transfer (absorption) coefficients prediction from data on heat transfer and fluid friction, Ind. Eng. Chem. 26 (1934) 1183–1187.

[46] O. Levenspiel, Chemical reaction engineering, Ind. Eng. Chem. Res. 38 (1999) 4140–4143.

[47] D. deMontigny, A. Aboudheir, P. Tontiwachwuthikul, A. Chakma, Modelling the performance of a CO_2 absorber containing structured packing, Ind. Eng. Chem. Res. 45 (2006) 2594–2600.

[48] A. Aboudheir, P. Tontiwachwuthikul, M. Wilson, R. Idem, Applications of New Absorption Kinetics and Vapor/Liquid Equilibrium Models to Simulation of a Pilot Plant for Carbon Dioxide Absorption Into High CO2-Loaded, Concentrated Aqueous Monoethanolamine Solutions. Submitted to, Sep. Purif. Technol. (2005).

[49] M.H. De Brito, U. Von Stockar, A.M. Bangerter, P. Bomio, M. Laso, Effective mass-transfer area in a pilot plant column equipped with structured packings and with ceramic rings, Ind. Eng. Chem. Res. 33 (1994) 647–656.

[50] B. Hanley, C.-C. Chen, New mass-transfer correlations for packed towers, AIChE J. 58 (2012) 132–152.

[51] J.A. Rocha, J.L. Bravo, J.R. Fair, Distillation columns containing structured packings: a comprehensive model for their performance. 2. Mass-transfer model, Ind. Eng. Chem. Res. 35 (1996) 1660–1667.

[52] J.A. Rocha, J.L. Bravo, J.R. Fair, Distillation columns containing structured packings: a comprehensive model for their performance. 1. Hydraulic models, Ind. Eng. Chem. Res. 32 (1993) 641–651.

[53] M.Z. Shahid, A.S. Maulud, M.A. Bustam, H. Suleman, Modeling of CO2-MEA absorption system in the packed column using Sulzer DX structured packing, in: Energy Secur. Chem. Eng. Congr., 2020.

[54] J.L. Bravo, J.A. Rocha, J.R. Fair, Mass transfer in gauze packings, Hydrocarb. Process. (International Ed.). 64 (1985) 91–95.

[55] T. Sema, A. Naami, Z. Liang, R. Idem, P. Tontiwachwuthikul, H. Shi, P. Wattanaphan, A. Henni, Analysis of reaction kinetics of CO_2 absorption into a novel reactive 4-diethylamino-2-butanol solvent, Chem. Eng. Sci. 81 (2012) 251–259.

[56] W.K. Lewis, W.G. Whitman, Principles of gas absorption, Ind. Eng. Chem. 16 (1924) 1215–1220.

[57] P.V. Danckwerts, A. Lannus, Gas-liquid reactions, J. Electrochem. Soc. 117 (1970) 369C.

[58] R. Higbie, The rate of absorption of a pure gas into a still liquid during short periods of exposure, Trans. AIChE. 31 (1935) 365–389.

[59] D.W. Van Krevelen, P.J. Hoftijzer, Kinetics of gas-liquid reactions part I. General theory, Recl. Des Trav. Chim. Des Pays-Bas. 67 (1948) 563–586.

[60] K.E. Porter, Effect of contact-time distribution on gas absorption with chemical reaction, Trans. Inst. Chem. Eng. Chem. Eng. 44 (1966) T25.

[61] R.M. Wellek, R.J. Brunson, F.H. Law, Enhancement factors for gas-absorption with second-order irreversible chemical reaction, Can. J. Chem. Eng. 56 (1978) 181–186.

[62] A.A. Yeramian, J.C. Gottifredi, J.J. Ronco, Mass transfer with homogeneous second order irreversible reaction a note on an explicit expression for the reaction factor, Chem. Eng. Sci. 25 (1970) 1622–1625.

[63] G. Astaria, D.W. Savage, A. Bisio, Gas treating with chemical solvents, (1983).

[64] M. Afkhamipour, M. Mofarahi, P. Pakzad, C.-H. Lee, Thermodynamic modelling of CO_2 absorption into aqueous solutions of 2-diethylaminoethanol, piperazine, and blended diethylaminoethanol with piperazine, Fluid Phase Equilib. 493 (2019), https://doi.org/10.1016/j.fluid.2019.02.008.

[65] P. Pakzad, M. Mofarahi, A.A. Izadpanah, M. Afkhamipour, Experimental data, thermodynamic and neural network modeling of CO_2 absorption capacity for 2-amino-2-methyl-1-propanol (AMP)+Methanol (MeOH)+H_2O system, J. Nat. Gas Sci. Eng. 73 (2020), 103060.

[66] A.L. Kohl, R.B. Nielsen, Gas Purification, Firth Edit, Houston, Texas Gulf Publ, Company, Houston, Texas, 1997.

[67] M. Afkhamipour, M. Mofarahi, Effects of operating parameters of packed columns on the KGav for CO2 absorption by amine solutions using optimization–simulation framework, Sep. Purif. Technol. 202 (2018) 86–102.

[68] P. Debye, E. Hückel, De la theorie des electrolytes. I. abaissement du point de congelation et phenomenes associes, Phys. Zeitschrift. 24 (1923) 185–206.

[69] P. Pakzad, M. Mofarahi, A.A. Izadpanah, M. Afkhamipour, C.-H. Lee, An experimental and modeling study of CO_2 solubility in a 2-amino-2-methyl-1-propanol (AMP)+N-methyl-2-pyrrolidone (NMP) solution, Chem. Eng. Sci. 175 (2018) 365–376.

[70] D.-Y. Peng, D.B. Robinson, A new two-constant equation of state, Ind. Eng. Chem. Fundam. 15 (1976) 59–64.

[71] H.M. Kvamsdal, G.T. Rochelle, Effects of the temperature bulge in CO_2 absorption from flue gas by aqueous monoethanolamine, Ind. Eng. Chem. Res. 47 (2008) 867–875.

[72] G.B. Liu, K.T. Yu, X.G. Yuan, C.J. Liu, Q.C. Guo, Simulations of chemical absorption in pilot-scale and industrial-scale packed columns by computational mass transfer, Chem. Eng. Sci. 61 (2006) 6511–6529.

[73] K. Maneeintr, A. Henni, R.O. Idem, P. Tontiwachwuthikul, A.G.H. Wee, Physical and transport properties of aqueous amino alcohol solutions for CO_2 capture from flue gas streams, Process Saf. Environ. Prot. 86 (2008) 291–295.

[74] F. Pouryousefi Dargah, Development of on-line analytical technique for determination of composition of CO2-loaded formulated amine solvents based on the liquid thermo physical properties for a post-combustion CO_2 capture process, faculty of graduate studies and research, University of Regina (2015).

[75] T. Sema, M. Edali, A. Naami, R. Idem, P. Tontiwachwuthikul, Solubility and diffusivity of N_2O in aqueous 4-(diethylamino)-2-butanol solutions for use in postcombustion CO2 capture, Ind. Eng. Chem. Res. 51 (2012) 925–930.

[76] G.F. Versteeg, W.P.M. van Swaaij, On the kinetics between CO_2 and alkanolamines both in aqueous and non-aqueous solutions-II. Tertiary amines, Chem. Eng. Sci. 43 (1988) 587–591.

[77] J.S. Cho, Gas absorption in a countercurrent packed tower:(1) Absorption with simultaneous chemical reaction (2) absorption into varying viscous solutions, (1987).

[78] T.J. Edwards, G. Maurer, J. Newman, J.M. Prausnitz, Vapor-liquid equilibria in multicomponent aqueous solutions of volatile weak electrolytes, AIChE J. 24 (1978) 966–976.

[79] A.R.I. Teerawat Sema, Paitoon Tontiwachwuthikul, Zhiwu Liang, Front-Edge Carbon Capture Technology: New Solvent Development, A Case Study of 4-Diethylamino-2-Butanol, 4th Korea CCS Int. Conf. (2014). http://www.koreaccs.or.kr/esub03_4_2/data/down/year/2014/page/3/id/610/num/1.

[80] F. Pouryousefi, Development of on-line analytical technique for determination of composition of CO2-loaded formulated amine solvents based on the liquid thermophysical properties for a post-combustion CO_2 capture process, PhD Thesis, University of Regina, Canada, 2015.

[81] R.H. Perry, D.W. Green, Perry's Chemical Engineers' Handbook 7 (2019) painos.

[82] R.C. Reid, J.M. Prausnitz, B.E. Poling, The properties of gases and liquids, (1987).